Kinetics of nanoring formation on surfaces of stressed thin films

Lin Du,[1] Mikhail Khenner,[2] and Dimitrios Maroudas[1,*]

[1]*Department of Chemical Engineering, University of Massachusetts, Amherst, Massachusetts 01003-9303, USA*

[2]*Department of Mathematics and Applied Physics Institute, Western Kentucky University, Bowling Green, Kentucky 42101, USA*

(Received 12 March 2018; published 13 August 2018)

We model the kinetics of nanoring (NR) formation in stressed thin films and explore systematically the resulting nanoring structures upon variation of the film thermal processing parameters. We find that the thermal stress induced in the films during their thermal annealing can trigger the transformation of quantum dots on the film surface to simple NRs or multiple concentric NRs. Our analysis provides a comprehensive explanation of experimentally observed nanoring formation on stressed film surfaces, as well as a design rule for fabricating NRs with precisely controlled features and sizes.

DOI: 10.1103/PhysRevMaterials.2.083403

I. INTRODUCTION

Solid material nanostructures in the form of nanorings (NRs) exhibit tunable plasmon resonance [1,2] and spin-polarized current switching [3,4] due to the unique nature of their electronic confinement and, thus, have the potential for use in numerous technological applications in optoelectronic [5,6] and magnetic data storage [7] devices. Various methods have been developed for the fabrication of NR structures [8–13], featuring the use of templates or the simultaneous diffusion of two atomic species and crystallization of two different materials. Recent experimental studies have demonstrated the formation of NRs from epitaxial nanoclusters or quantum dots (QDs) on pure gold [14] and silver [15] films deposited on oxide substrates; this QD-NR transition occurs simply upon thermal annealing.

Theoretical energetic analyses have revealed that the formation of NRs from QDs during thermal annealing is due to the release of the increased elastic strain energy in the film, accumulated due to its thermal mismatch with the substrate, and have showed that the NR structure is a thermodynamically favorable configuration [16,17]. Formation of NRs and complex quantum dot molecules (QDMs) also has been predicted in the studies of possible steady-state morphologies for QDs with various sizes by using a thermodynamic model [18]. However, the fundamental kinetics of the QD-NR transition upon thermal annealing of stressed films remains unexplored.

Kinetic models for the surface morphological evolution of solid materials driven by surface diffusion have predicted successfully and explained pattern-formation phenomena on stressed film surfaces [19–23], including the formation of QDMs in strained-layer epitaxy [23]. In this study, we conduct a kinetic analysis of surface morphological evolution in stressed thin films under thermal annealing, which captures the NR formation dynamics and explains the QD-NR transition. The analysis also provides design rules for developing NR structures with precisely controlled features and sizes.

The rest of the article is structured as follows: The kinetic model of the morphological evolution of the film surface and the computational methods employed to simulate the kinetics of nanoring formation on the surface of the stressed film are described and discussed in Sec. II. The simulation results are presented in Sec. III, revealing transformation of quantum dots to nanorings as well as formation of multiple concentric nanorings depending on the film thermal processing parameters. The simulation results are discussed and analyzed on the basis of morphological stability theory in Sec. IV. Finally, the main conclusions of our study are summarized in Sec. V.

II. MODEL AND COMPUTATIONAL METHODS

We consider a thin film deposited on a rigid substrate with a nominal film thickness of h_0, as depicted in Fig. 1(a). The material of the film is different from that of the substrate and the two materials have different equilibrium densities. As a result of this volume mismatch, the film is subjected to an equibiaxial compressive stress, with stress components $\sigma_{xx} = \sigma_{yy} = \sigma_0$ in the x and y directions, respectively, of a Cartesian frame of reference. Assuming that σ_0 is less than the yield stress of the crystalline film material, we neglect plastic deformation phenomena in the film. Parametrizing the film surface morphology with the surface height function $h(x, y, t)$, the film surface morphological evolution can be described by the continuity equation

$$\frac{\partial h}{\partial t} = H' \nabla_s \cdot \left[\frac{\delta_s \Omega D_s}{k_B T} \nabla_s (U_E - \gamma_f \kappa + U_W) \right]. \quad (1)$$

In Eq. (1), $H' \equiv (1 + h_x^2 + h_y^2)^{1/2}$, $h_x \equiv \frac{\partial h}{\partial x}$, $h_y \equiv \frac{\partial h}{\partial y}$, Ω is the atomic volume, δ_s/Ω is the number of surface atoms per unit area, k_B is the Boltzmann constant, T is temperature, D_s is the surface atomic diffusivity, and ∇_s represents the surface gradient operator, acting within the brackets in the right-hand side of Eq. (1) on the chemical potential of the film surface atoms. The latter includes contributions from the densities of the elastic strain energy U_E; the surface energy $\gamma_f \kappa$, where γ_f is the surface free energy per unit area of the film and κ is

*maroudas@ecs.umass.edu

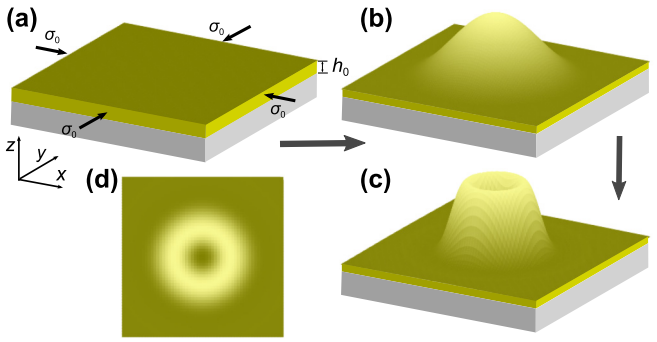

FIG. 1. Schematic representation of the morphological evolution of a biaxially stressed thin film surface from (a) planar to (b) a three-dimensional island (QD) and to (c) a nanoring structure upon thermal annealing, with the top view of the nanoring structure shown in panel (d).

the film surface curvature; and the wetting potential, U_W. The wetting potential density is described by the "transition-layer" (of thickness b) model [24,25],

$$U_W = (\gamma_f - \gamma_s)b/[H'\pi(b^2 + h^2)], \tag{2}$$

where γ_s is the surface free energy per unit area of the substrate.

In the above film surface evolution model, the effects of surface crystallographic orientation are neglected and both the surface diffusivity and the surface free energy are assumed to be isotropic; surface property anisotropies are not expected to have any major effect on the kinetics of film surface morphological evolution, which is mainly affected by the magnitude of the stress in the film. Also, desorption from the film surface is neglected given the typical thicknesses and temperatures of the films considered here. U_E is computed by solving the elastostatic boundary-value problem (BVP) in the film and calculating the stress and strain tensors at every point on the film surface [26].

Dimensional analysis of Eq. (1) gives a length scale $l \equiv \frac{M_s\gamma_f}{\sigma_0^2}$, where M_s is the biaxial modulus of the substrate [23], a time scale $\tau \equiv \frac{k_B T l^4}{\delta_s \Omega D_s \gamma_f}$, and a dimensionless parameter $\Xi_W = [2b(\gamma_s - \gamma_f)/(\pi h_o^3 \gamma_f)]l^2$ that expresses the strength of the wetting potential [26]. Finally, we emphasize that the film and substrate materials also are thermally mismatched, i.e., the two materials have different thermal expansion coefficients, β_f and β_s, respectively, and focus on the case where $\beta_f > \beta_s$, such as in the Ag/quartz film/substrate system.

To explore the kinetics of the stressed film surface morphological evolution, we conduct systematic dynamical simulations according to the film evolution model of Eq. (1). In the simulations, we solve the elastostatic BVP self-consistently with the film surface propagation based on a spectral collocation method [25], where the film surface is discretized by using 128×128 grid points, and discrete fast Fourier transforms are performed. For the integration of Eq. (1), we employ an advanced operator splitting-based semi-implicit spectral method [27] with adaptive time-step size.

We first perturb a planar film surface, such as that shown in Fig. 1(a), and let the surface evolve until it reaches a steady state. The stressed film surface undergoes a Stranski–Krastanow (SK) morphological instability and evolves into a stable pattern of QDs arranged periodically on the surface; the unit cell of the periodic QD pattern is depicted schematically in Fig. 1(b). Subsequently, starting from this regular array of QDs, as the initial film surface morphology, we increase the biaxial stress level σ_0 in the film by a factor of α that is directly proportional to the temperature increase ΔT in the thermal annealing process,

$$\alpha \equiv 1 + (\beta_f - \beta_s)E_f \Delta T/[(1 - \nu_f)\sigma_0], \tag{3}$$

and continue the dynamical simulation. In Eq. (3), E_f and ν_f are the Young's modulus and Poisson ratio of the film, respectively, σ_0 is the biaxial stress level in the film prior to its thermal annealing, and $\alpha - 1$ represents the dimensionless thermal stress induced in the film upon thermal annealing (scaled with σ_0).

III. SIMULATION RESULTS

Representative configurations from our simulations of the evolving film surface morphology during the thermal annealing process for $\alpha = 2.0$, $\alpha = 2.4$, and $\alpha = 2.8$ are shown in Figs. 2(a1)–2(a6), 2(b1)–2(b6), and 2(c1)–2(c6), respectively. Using the Ag/quartz system as a representative material system and the deposition conditions in Ref. [15], the length scale l and the time scale τ are estimated to be 90 nm and 6 h, respectively.

Figure 2(a1) shows the top view of a QD with a diameter of ~360 nm. As seen in Fig. 2(a2), under the action of the increased biaxial stress at $\alpha = 2.0$ due to thermal annealing, the diameter of the QD shrinks. More interestingly, as a result of the increased stress, the QD undergoes a morphological transition, characterized by morphological modulation in the radial direction. Moreover, the flat wetting layer undergoes an analogous morphological modulation as a means of relieving the increased elastic strain energy. Figure 2(a3) shows that the modulated QD gradually evolves into a ring structure with a narrower QD at the ring center. This type of surface morphological feature also was predicted by the energetic model and observed experimentally [18]. A larger-diameter ring also is formed by the material in the wetting layer. However, this ring is not as tall as the central ring and breaks into numerous small QDs symmetrically arranged with respect to the principal biaxial stress axes; namely, the x and y axes of the Cartesian frame of reference. As shown in Fig. 2(a4), the narrow central QD eventually vanishes, leaving a symmetric ring structure, which resembles strongly both the gold NRs in Ref. [14] and the silver NR in Ref. [15].

In Fig. 2(a5), the cross-sectional profile of the NR in Fig. 2(a4) is compared with that of the initial QD in Fig. 2(a1); both profiles, in red and blue, respectively, are along a horizontal line (parallel to the x axis) that goes through the unit cell's center. The NR height is about twice that of the original QD, while the underneath wetting layer is much thinner than that in the original QD configuration. The heights of the nanostructures are constrained by the amount of the film material available, satisfying conservation of mass. Consequently, the height and the width of the NR structures can be precisely controlled by controlling the amount of film material deposited on the substrate prior to its thermal annealing.

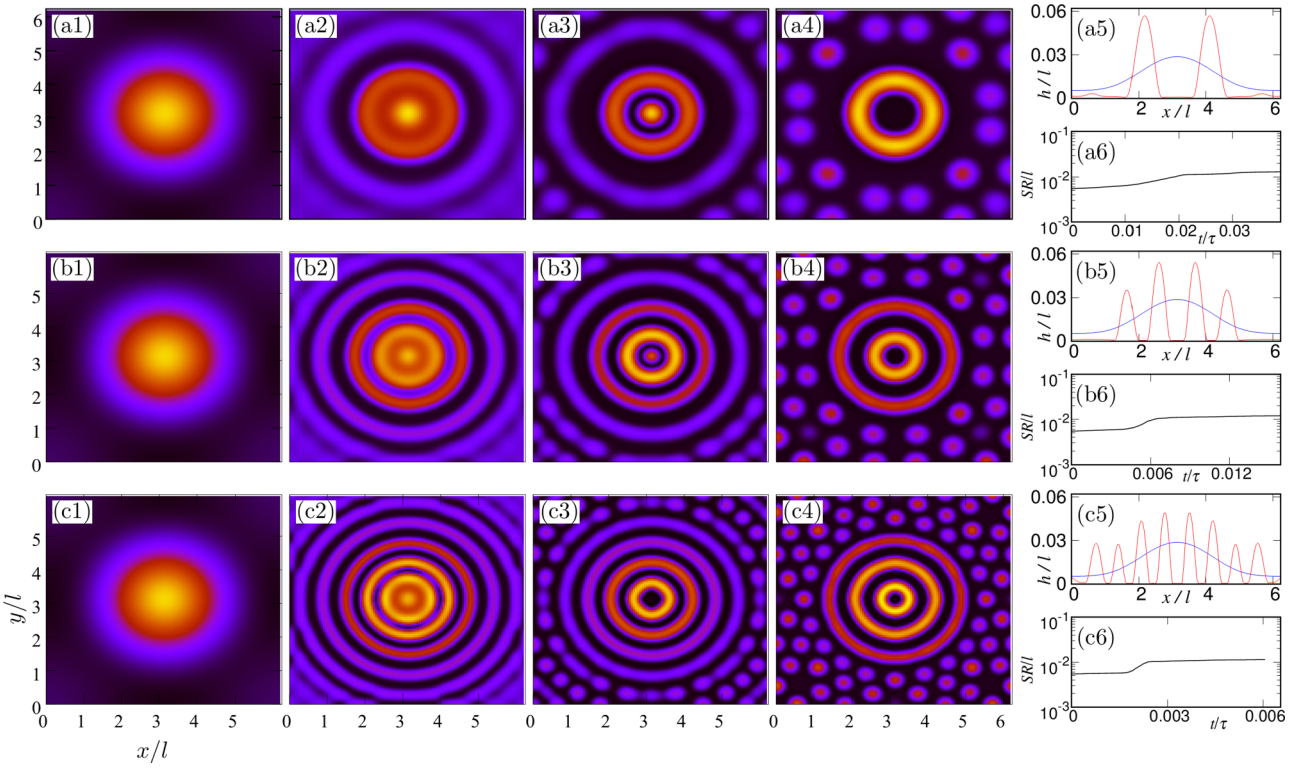

FIG. 2. Two-dimensional contour maps of simulated evolving surface morphology, $h(x, y, t)$, upon thermal annealing of a biaxially stressed thin film starting with an equilibrium surface morphology that consists of a periodic arrangement of quantum dots (QDs), with (a1), (b1), (c1) the top view of one such QD structure shown in the unit cell of the post-SK-instability regular QD pattern for (a1)–(a6) $\alpha = 2.0$ at (a1) $t = 0$, (a2) $t = 1.52 \times 10^{-2}\tau$, (a3) $t = 2.32 \times 10^{-2}\tau$, and (a4) $t = 3.92 \times 10^{-2}\tau$; (b1)–(b6) $\alpha = 2.4$ at (b1) $t = 0$, (b2) $t = 0.54 \times 10^{-2}\tau$, (b3) $t = 0.69 \times 10^{-2}\tau$, and (b4) $t = 1.59 \times 10^{-2}\tau$; and (c1)–(c6) $\alpha = 2.8$ at (c1) $t = 0$, (c2) $t = 0.220 \times 10^{-2}\tau$, (c3) $t = 0.326 \times 10^{-2}\tau$, and (c4) $t = 0.606 \times 10^{-2}\tau$. One-dimensional surface profiles $h(x; y, t)$ along the x direction and passing through the center of the unit cell of (a1) and (a4), (b1) and (b4), and (c1) and (c4) are plotted in blue and red, respectively, in (a5), (b5), and (c5), respectively. The simulated evolution of the film surface rms roughness, SR, in cases (a1)–(a4), (b1)–(b4), and (c1)–(c4) is plotted in panels (a6), (b6), and (c6), respectively. In the simulations, $h_0 = 0.009l$ and $\Xi_W = 0.873$.

The most interesting feature of the formed NR configuration is its radius, determined by the competition of the different driving forces for mass transport. It is worth noting that the NR structure is energetically more favorable and, thus, can retain its morphology for longer time compared with intermediate structures, such as that shown in Fig. 2(a3). This also is shown in the plot of the surface rms roughness, SR, evolution [28] in Fig. 2(a6). The roughness increase in the short time period between about 0.01 and 0.023τ marks the onset of the morphological transformation from QD to NR. The long-time plateau in the SR evolution after the NR formation (see the supplementary material [26]) shows that the NR structure is indeed a (metastable) asymptotic state reached in the evolution of the surface morphology of the further stressed film upon thermal annealing. This explains why NR structures are easy to be observed in the thermal annealing experiments of such deposited thin films [14,15]. As discussed in the supplementary material [26], the NR structure of Fig. 2(a4) is metastable, and eventually breaks into a cluster of four closely located and symmetrically arranged QDs forming a QDM. This NR metastability also agrees with the experimental observation that increasing the duration of the films' thermal annealing causes a decrease of the observed number of NRs in the films [14].

According to Eq. (3), α can be tuned precisely by changing the film and substrate materials with different thermal expansion coefficients or by varying the thermal annealing temperature. Being able to tune α, it is worth exploring other interesting surface nanostructures that may be generated by thermal annealing of such stressed thin films. Such nanostructures include multiple concentric NRs. Figures 2(b1)–2(b4) show the evolution of the same initial QD structure into a double concentric NR for $\alpha = 2.4$, i.e., for biaxial stress level $\sigma = 2.4\sigma_0$ in the film. As seen in Fig. 2(b5), the inner and outer ring in this double concentric NR configuration have diameters of $\sim 1.08l$ and $\sim 2.94l$, respectively. Similarly, Figs. 2(c1)–2(c4) show the evolution of the QD structure into a triple concentric NR for $\alpha = 2.8$. As seen in Fig. 2(c5), in this triple concentric NR configuration, the diameters of the inner, the middle, and the outer ring are $\sim 0.78l$, $\sim 2.16l$, and $\sim 3.53l$, respectively. Figures 2(b6) and 2(c6) show clearly the short time period required for the morphological transformation to reach the asymptotic states of the double and triple, respectively, NR structures. Similarly to the single NR case, as shown in the supplementary material [26], these double and triple concentric NRs eventually break into QDs and form regular QDM patterns.

Figure 2 shows that the stress increase induced by the thermal mismatch between the film and the substrate in the thermal annealing process can trigger further evolution of the equilibrium QD pattern to transform into a NR pattern. It also shows that tuning the parameter α can lead to the formation of different multiple concentric NR structures. Our simulations reveal that if α is not sufficiently large, the QD will not transform into a NR structure. Indeed, as shown in the supplementary material [26], there is a critical value of α, $\alpha_c \approx 1.53$, that marks the onset of the QD-NR transition. In brief, our simulations demonstrate that the number of concentric NRs formed per QD, n_{NR}, can be controlled by controlling the increase in the biaxial stress in the film, by the additional thermal stress due to thermal annealing, as expressed by the parameter α.

IV. MORPHOLOGICAL STABILITY THEORY

It is evident from Figs. 2(a1)–2(a4), 2(b1)–2(b4), and 2(c1)–2(c4) that the morphology of the QD during the film surface morphological evolution remains axially symmetric with the morphological changes occurring only in the radial direction. This observation allows us to focus our analysis on the changes in the cross-sectional profiles of the nanostructures shown in Figs. 2(a5), 2(b5), and 2(c5). The evolution of these profiles implies that the film surface undergoes a tip-splitting instability in the radial direction, which is similar in nature to the instability of the surfaces of uniaxially stressed solids [29]. In previous studies, we developed a theory for the nonlinear tip-splitting phenomena that can be triggered by long-wavelength plane-wave perturbations [23,29]. In an analogous manner, the original QD profile can be viewed as a long-wavelength perturbation, with a dimensionless perturbation wavelength $\tilde{\lambda} = 2\tilde{R}$, where $\tilde{R}$ is the dimensionless QD radius, with both lengths made dimensionless by the dynamic length scale, l, of the film/substrate material system.

Following the analysis of Ref. [29], we derive (see the supplementary material [26]) the relation between $\tilde{R}$ and the number of ripples, n, that the QD profile can split into,

$$\frac{\xi(n-1)\pi}{1+\zeta(n-1)} \leqslant \tilde{R} \leqslant \frac{\xi(n)\pi}{1+\zeta(n)}, \tag{4}$$

where $\xi(n) \equiv [(n+1)^4 - n^4]/[(n+1)^3 - n^3]$ and

$$\zeta(n) \equiv \sqrt{1 - \frac{[(n+1)^4 - n^4][(n+1)^2 - n^2]}{[(n+1)^3 - n^3]^2}\,\Xi_W}.$$

Obviously, $n = 1$ corresponds to the QD structure, $n = 2$ corresponds to the single NR structure, and $n = 3$ corresponds to a NR structure with a single narrow QD at the center, as seen in Fig. 2(a3). Although the dimensional radius of a QD, R, does not change after its morphology reaches a steady state, as the temperature increases, the thermal stress is induced and the total biaxial stress level increases by a factor of α, making the dynamic length scale, $l \equiv \frac{M_s \gamma_f}{\sigma_0^2}$, decrease by a factor of α^2; as a result, $\tilde{R}$ increases by a factor of α^2. If the resulting $\tilde{R}$ is sufficiently large, a tip-splitting instability will occur and a NR or multiple concentric NRs will form. Consistent with our analysis, the different asymptotic-state morphologies for QDs with different sizes also were predicted in Ref. [18].

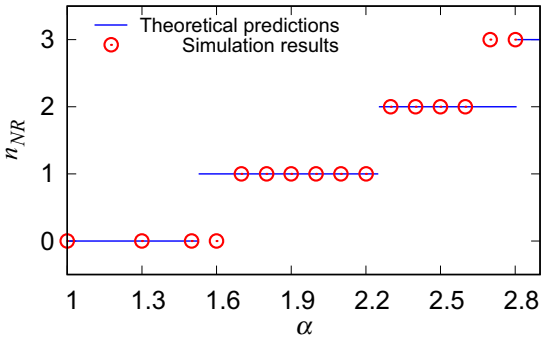

FIG. 3. Number of concentric nanorings, n_{NR}, formed per QD of the surface of a thermally annealed biaxially stressed thin film, consisting prior to annealing of a periodic QD pattern, as a function of the film biaxial stress level increase factor α. Solid lines and open circles denote theoretical predictions and simulation results, respectively. The processing conditions are the same with those in Fig. 2.

Since we are only interested in the (meta)stable NR structures and the structure depicted in Fig. 2(a3) quickly evolves into a single NR, $n = 3$ also yields a single late-time NR structure. In general, the relation between n and n_{NR}, the number of late-time NRs, is

$$n_{NR} = [n/2], \tag{5}$$

where $[\cdot]$ denotes the integer part, i.e., $[3/2] = 1$, $[5/2] = 2$, etc. Equations (4) and (5) provide a quantitative relation between $\tilde{R}$ and the late-time number of concentric NRs, n_{NR}, in a generally multiple concentric NR configuration that may form as a result of the thermal annealing of the deposited film.

To validate the above theory, we conducted a systematic protocol of numerical simulations by using the same conditions as those in Fig. 2, with α varying over the range from 1.0 to 2.8. The initial QD has a dimensionless radius of $\sim$2, as seen in Fig. 2(a5). In the thermal annealing process, with the increase of the biaxial stress level in the film, the dimensionless QD radius becomes $\tilde{R} \sim 2\alpha^2$. In each simulation, we count the number of the formed concentric NRs, n_{NR}. The simulation results are plotted in Fig. 3 as open circles and are compared with the theoretical predictions (4) and (5) represented by the piecewise continuous (staircase) function consisting of the blue line segments. The theoretical predictions are in very good agreement with the simulation results, thereby validating the theory of NR formation as the outcome of a nonlinear stress-driven tip-splitting morphological instability.

V. SUMMARY AND CONCLUSIONS

In conclusion, our modeling results provide a fundamental kinetic interpretation of the experimental reports in the literature on nanoring pattern formation in stressed deposited films and determine the effects on NR formation of all the relevant processing conditions and material parameters. Our dynamical simulations demonstrate that multiple concentric NRs can form from sufficiently large QDs at sufficiently high annealing temperatures. We have also provided a fundamental theoretical explanation of NR formation, which serves as a design rule for developing NR patterns on stressed film surfaces

as well. It should be realized that, although these NR patterns are metastable, their formation kinetics is diffusion controlled; therefore, lowering the temperature can diminish the diffusion rates and "freeze" these patterns in place.

It should be mentioned that our model is applicable to a variety of film/substrate systems, including epitaxial material systems, such as Ge/Si and SiGe/Si; however, we emphasize that, for NR formation through a QD-NR transition upon thermal annealing, the most suitable material systems are those characterized by a substantial thermal mismatch between the film and the substrate materials, such as the metal/oxide systems used in Refs. [14,15]. Moreover, in principle, our model can be used to determine material parameters; namely, thermal expansion coefficients and elastic moduli, by combining the findings of our study for the onset of NR and multiple concentric NR formation [results of Fig. 3 and/or Eqs. (4) and (5)] with Eq. (3) for the thermal stress in the film during thermal annealing at given annealing temperatures.

ACKNOWLEDGMENTS

D.M. and L.D. acknowledge support by the U.S. Department of Energy, Office of Basic Energy Sciences, Division of Materials Sciences and Engineering, under Award No. DE-FG02-07ER46407. M.K. acknowledges support by NSF KY EPSCoR (Grant No. 3200000271-18-069) and by the Western Kentucky University Research Foundation (QTAG grant).

[1] X. Fang, Z. Li, Y. Long, H. Wei, R. Liu, J. Ma, M. Kamran, H. Zhao, X. Han, B. Zhao, and X. Qiu, Phys. Rev. Lett. **99**, 066805 (2007).
[2] T. Kelf, Y. Tanaka, O. Matsuda, E. Larsson, D. S. Sutherland, and O. Wright, Nano Lett. **11**, 3893 (2011).
[3] A. Lorke, R. J. Luyken, A. O. Govorov, J. P. Kotthaus, J. M. Garcia, and P. M. Petroff, Phys. Rev. Lett. **84**, 2223 (2000).
[4] A. Fuhrer, S. Lüscher, T. Ihn, T. Heinzel, K. Ensslin, W. Wegscheider, and M. Bichler, Nature (London) **413**, 822 (2001).
[5] C. Huang, J. Ye, S. Wang, T. Stakenborg, and L. Lagae, Appl. Phys. Lett. **100**, 173114 (2012).
[6] J. Aizpurua, P. Hanarp, D. S. Sutherland, M. Käll, G. W. Bryant, and F. G. García de Abajo, Phys. Rev. Lett. **90**, 057401 (2003).
[7] L. W. Yu, K. J. Chen, J. Song, J. Xu, W. Li, X. F. Li, J. M. Wang, and X. F. Huang, Phys. Rev. Lett. **98**, 166102 (2007).
[8] K. L. Hobbs, P. R. Larson, G. D. Lian, J. C. Keay, and M. B. Johnson, Nano Lett. **4**, 167 (2004).
[9] T. Mano, T. Kuroda, S. Sanguinetti, T. Ochiai, T. Tateno, J. Kim, T. Noda, M. Kawabe, K. Sakoda, G. Kido, and N. Koguchi, Nano Lett. **5**, 425 (2005).
[10] T. Kuroda, T. Mano, T. Ochiai, S. Sanguinetti, K. Sakoda, G. Kido, and N. Koguchi, Phys. Rev. B **72**, 205301 (2005).
[11] E. M. Larsson, J. Alegret, M. Käll, and D. S. Sutherland, Nano Lett. **7**, 1256 (2007).
[12] C. Somaschini, S. Bietti, N. Koguchi, and S. Sanguinetti, Nano Lett. **9**, 3419 (2009).
[13] O. K. Zahr and A. S. Blum, Nano Lett. **12**, 629 (2012).
[14] F. Ruffino, I. Crupi, F. Simone, and M. Grimaldi, Appl. Phys. Lett. **98**, 023101 (2011).
[15] Y. Mishra, R. Adelung, G. Kumar, M. Elbahri, S. Mohapatra, R. Singhal, A. Tripathi, and D. Avasthi, Plasmonics **8**, 811 (2013).
[16] S. P. A. Gill, J. Appl. Phys. **113**, 154316 (2013).
[17] S. P. A. Gill, J. Mech. Phys. Solids **78**, 94 (2015).
[18] L. Shanahan and B. J. Spencer, Interface. Free Bound. **4**, 1 (2002).
[19] W. H. Yang and D. J. Srolovitz, Phys. Rev. Lett. **71**, 1593 (1993).
[20] J. Tersoff and F. K. LeGoues, Phys. Rev. Lett. **72**, 3570 (1994).
[21] Y. Pang and R. Huang, J. Appl. Phys. **101**, 023519 (2007).
[22] V. Tomar, M. R. Gungor, and D. Maroudas, Phys. Rev. Lett. **100**, 036106 (2008).
[23] L. Du and D. Maroudas, Appl. Phys. Lett. **109**, 023103 (2016).
[24] B. J. Spencer, Phys. Rev. B **59**, 2011 (1999).
[25] Y. Pang and R. Huang, Phys. Rev. B **74**, 075413 (2006).
[26] See Supplemental Material at http://link.aps.org/supplemental/10.1103/PhysRevMaterials.2.083403 for the evolution of the metastable nanoring structures to form quantum dot clusters and the derivation of the morphological stability theory that provides the basis for the theory of multiple concentric nanoring formation.
[27] G. Tegze, G. Bansel, G. I. Tóth, T. Pusztai, Z. Fan, and L. Gránásy, J. Comput. Phys. **228**, 1612 (2009).
[28] L. Du and D. Maroudas, Appl. Phys. Lett. **110**, 103103 (2017).
[29] L. Du, D. Dasgupta, and D. Maroudas, J. Appl. Phys. **118**, 035303 (2015).